Atmospheric Environment 206 (2019) 108–118

Contents lists available at ScienceDirect

Atmospheric Environment

journal homepage: www.elsevier.com/locate/atmosenv

Is the biosphere-atmosphere exchange of total reactive nitrogen above forest driven by the same factors as carbon dioxide? An analysis using artificial neural networks

Undine Zöll[a], Antje M. Lucas-Moffat[a,b], Pascal Wintjen[a], Frederik Schrader[a], Burkhard Beudert[c], Christian Brümmer[a,*]

[a] Thünen Institute of Climate-Smart Agriculture, Bundesallee 65, 38116, Braunschweig, Germany
[b] Also at German Meteorological Service, Centre for Agrometeorological Research, Bundesallee 33, 38116, Braunschweig, Germany
[c] Bavarian Forest National Park, 94481, Grafenau, Germany

ARTICLE INFO

Keywords:
Total reactive nitrogen
Eddy covariance
CO_2
Forest
Artificial neural networks

ABSTRACT

Phase and amplitude of ecosystem-atmosphere fluxes of reactive nitrogen compounds are poorly understood due to a lack of suitable observation methods. Understanding the biophysical controls of the surface nitrogen exchange is essential for the parameterization of process-based and chemical transport models that can be used for the determination of regional or national nitrogen budgets. In this study, we investigated similarities in time series of net total reactive nitrogen (ΣN_r) and carbon dioxide (CO_2) fluxes above forest with regard to their variability and driving factors. We found corresponding shapes of the mean diurnal summertime patterns of ΣN_r and CO_2. While ecosystem respiration leads to a net CO_2 release at night, ΣN_r was on average deposited throughout the entire observation period. Using artificial neural network analysis, global radiation (R_g) was identified to be the main control for both ΣN_r and CO_2. While the concentration of ΣN_r substantially improved the coefficient of determination for ΣN_r fluxes when used as a secondary driver, only minor improvements of 2–3% were found for CO_2 fluxes when using for example temperature or vapour pressure deficit (VPD) as secondary driver. Considering two dominant drivers, 41 and 66% of the variability in ΣN_r and CO_2 fluxes, respectively, could be explained. Further data stratification for ΣN_r revealed that higher concentrations, higher temperature, and higher VPD as well as dry leaf surfaces tend to favour higher deposition of ΣN_r, whereas lower concentrations, lower temperature, and lower VPD as well as wet leaf surfaces mainly correspond to situations when less ΣN_r was deposited or even emitted. Our results support the understanding of biosphere-atmosphere interactions, their driving factors, and establish a link between ΣN_r and CO_2 exchange, which may be beneficial for future developments in state-of-the-art exchange modelling.

1. Introduction

Nitrogen is a key element on earth. As elemental nitrogen (N_2) it makes up 78% of the atmosphere. In the biosphere its reactive forms play a major role for plant growth (Follett and Hatfield, 2001). While it can be a limiting factor in natural ecosystems, an excessive supply of nitrogen through synthetic fertilization or atmospheric deposition can lead to a number of harmful effects, such as eutrophication of ecosystems or adverse effects on human health (Erisman et al., 2013). In an agricultural context, ammonia (NH_3) plays a special role: While it readily deposits to all kinds of (especially wet) surfaces, it also underlies bi-directional exchange and can be emitted from agriculturally used areas, from fertilized fields as well as animal housings, stored manure or the like (Sutton et al., 2011; Flechard et al., 2013), as well as from natural ecosystems with a history of high N deposition (Farquhar et al., 1980). Nitrogen oxides, on the other hand, are mainly emitted from the industry and transportation sector (Sutton et al., 2011; Fowler et al., 2013). NO and NO_2 underlie photochemical reactions, during which NO_2 is photolyzed to NO, O_3 is formed, which reacts again with NO during the night to NO_2. In further steps NO_2 can react with O_3 to NO_3, NO_3 with NO_2 to N_2O_5, which can react with water to HNO_3. The latter, however, is mainly being formed through the reaction of NO_2 and OH radicals (Seinfeld and Pandis, 1997). In this study, the term NO_x refers to NO and NO_2 only, since these are the main NO_x compounds. The reduced N compounds can react to acidic (nitric acid and nitrous acid) or particulate compounds (ammonium and nitrates), and can play a role

* Corresponding author.
E-mail address: christian.bruemmer@thuenen.de (C. Brümmer).

https://doi.org/10.1016/j.atmosenv.2019.02.042
Received 20 August 2018; Received in revised form 21 February 2019; Accepted 24 February 2019
Available online 05 March 2019

in the formation of organic compounds such as amines and nitrates (e.g. peroxyacetyl nitrate). The above listed reactive nitrogen species are all together described as total reactive atmospheric nitrogen (ΣN_r) (Marx et al., 2012). Concentrations of those compounds are usually low, but near sources like stables, industry plants or busy streets critically high concentrations (i.e. mean annual above 21 ppb, hourly means above 106 ppb for NO_2, WHO, 2006; maximum allowed concentration of 18 ppm for NH_3, Erisman et al., 2013) and therewith high deposition rates can be reached. Those high concentrations threaten the health of humans regarding the respiratory system. Plants are more prone to stress factors such as frost and direct foliar damage can occur, but also whole ecosystems suffer from acidification, eutrophication, and generally decreasing species richness (Erisman et al., 2013).

Most campaigns on gaseous reactive nitrogen focus on NH_3 at agricultural sites as estimations of nitrogen losses from fertilizer applications suffer from considerable uncertainties in the measured fluxes (e.g., Sutton et al., 2009; Spirig et al., 2010). Historically widely used measurement techniques like passive samplers (Tang et al., 2009) and wet-chemistry analysers like AMANDA or AiRRmonia (von Bobrutzki et al., 2010) were operated at comparably low sampling frequencies with sometimes high detection limits, requiring modelling approaches to estimate exchange fluxes. Nowadays faster, more accurate and precise devices (e.g., quantum cascade lasers (Zöll et al., 2016), total reactive atmospheric nitrogen converter (TRANC) coupled to a chemiluminescense detector (Ammann et al., 2012), differential optical absorption spectroscopy (miniDOAS; Sintermann et al., 2016)) allow detecting low background concentrations and investigating driving variables other than ambient concentrations. With some of these devices, it is possible to apply the eddy-covariance (EC) method to derive exchange fluxes as it is common practice e.g. for carbon dioxide (CO_2) exchange. There are only few reactive nitrogen exchange measurement campaigns above forests, which mainly focus on one or only a few selected reactive nitrogen compounds under a variety of conditions with regard to e.g. wetness (e.g., Wyers and Erisman, 1998; Wolff et al., 2010; Geddes and Murphy, 2014; Hansen et al., 2015). The study here presented is the first one where all reactive nitrogen compounds were measured with a single analytical device coupled to the TRANC converter and using the eddy-covariance method to calculate biosphere-atmosphere exchange fluxes. Measurements were conducted in the Bavarian Forest National Park, which is located in rural counties of more than 57% woodland with a current population density of 80 km^{-2} on the German and less than 45 km^{-2} on the Czech side of this low mountain range (Beudert et al., 2018). There are no industries or power plants, which is demonstrated by low annual concentrations of NO_2 (2.9 ppb ± 0.7 ppb; data provided by the Bavarian Forest National Park, 1992–2017) and of NH_3 (1.4 ppb, 2003–2005; Beudert and Breit, 2010). Thereby this site offers the chance to measure background exchange and to investigate the natural interaction of ΣN_r with biophysical variables. However, this mixed ΣN_r signal is challenging to interpret because of different exchange behaviors mentioned briefly above. ΣN_r consists mainly of NO_2 and NH_3 (together at least 75% in Marx et al., 2012). Hurkuck et al. (2014) found that 80% of ΣN_r deposited to a semi-natural peatland site in close vicinity to agriculture consisted of NH_3. While the composition at a natural forest site might be different, we still assume NH_3 and NO_x to dominate the total ΣN_r exchange. According to our DELTA-Denuder measurements on average 33% of ΣN_r were NH_3 and 32% were NO_2 (measured separately by a chemiluminescence detector).

Usually reactive nitrogen concentrations are the primary driver for the exchange flux, but also other climatic drivers have an, mostly minor, effect (Milford et al., 2001; Flechard and Fowler, 1998; Zöll et al., 2016). Those rather small effects are difficult to disentangle because of interrelations between the drivers (Milford, 2004) and are not completely understood until now (Flechard et al., 2013). In contrast, CO_2 exchange has been widely researched and the main drivers, radiation and temperature, are well known (e.g. Chen et al., 2009).

Since there are no simple linear relationships between the ΣN_r fluxes and other environmental factors, such as temperature, relative humidity (RH) or global radiation (R_g, e.g., Milford et al., 2001), we aim to investigate the importance of certain biophysical factors for explaining the variability in ΣN_r fluxes by using artificial neural networks (ANNs). This method is widely used and has been successfully applied in an ecological context for explaining CO_2 exchange (Albert et al., 2017; Moffat et al., 2010; Park et al., 2018).

The aims of our study are to (1) investigate whether similarities in the diurnal flux patterns of CO_2 and ΣN_r exist, and if so, (2) whether these flux patterns are driven by the same or by different biophysical factors. Further, (3) we quantify the specific contribution of each controlling factor by using artificial neural network analysis to help improve our understanding of reactive nitrogen exchange mechanisms in natural forest ecosystems.

2. Materials and methods

2.1. Site description and local climate

To measure background total reactive nitrogen (ΣN_r) concentrations and fluxes, a remote site in the Bavarian Forest National Park, Germany (48°56′N 13°25′E, 807 m a.s.l., for a map see Fig. S1 in the supplements), some kilometers away from moderate anthropogenic emission sources, was chosen. The unmanaged site is located in a natural mixed forest stand in the Forellenbach catchment, which is a part of the International Cooperative Program on Integrated Monitoring of Air Pollution Effects on Ecosystems (ICP IM) within the framework of the Geneva Convention on Long-Range Transboundary Air Pollution (http://www.unece.org/env/lrtap/). Additionally, the Bavarian Forest National Park is part of the Long Term Ecological Research (LTER) network (for more details on the sites and data availability see https://data.lter-europe.net/deims/site/lter_eu_de_015). The stand mainly consists of spruce (*Picea abies*) and to approx. 20% of beech (*Fagus sylvatica*) species within the flux footprint. During the campaign, the stand reached only up to a height of 20 m, because it is recovering from a bark beetle outbreak in the mid-1990s and 2000s (Beudert et al., 2014). Annual mean air temperature at the site is 6.6 °C and the mean annual precipitation sum is 1563 mm per year (data provided by the Bavarian Forest National Park, 1978–2017).

2.2. Measurement setup

The 50 m high tower at the measurement site was set up in the 1980s and has been used for several measurement purposes, e.g. for nitrogen oxides (NO and NO_2), sulphur dioxide, and ozone monitoring within the framework of UN ECE IM on behalf of the German Environment Agency (UBA, Beudert and Gietl, 2015). In October 2015, we started to set up several instruments for a ΣN_r and CO_2 flux measurement campaign. Reliable fast response ΣN_r concentrations in an EC setup were recorded from summer 2016. Data from 14 July until 30 September were used for the analysis.

The setup consisted of a custom-built ΣN_r converter (total reactive atmospheric nitrogen converter (TRANC), after Marx et al., 2012), mounted on a boom at a height of 30 m above ground, as well as a chemiluminescence detector (CLD 780 TR, ECO PHYSICS AG, Dürnten, Switzerland) and a dry vacuum scroll pump (BOC Edwards XDS10, Sussex, UK), both situated on ground level. The sample path through the TRANC includes two main conversion steps: a heated iron-nickel-chrome (FeNiCr) alloy tube (approx. 870 °C) and a passively heated gold tube (approx. 300 °C). Carbon monoxide is added as a reducing agent after the sample air passed the FeNiCr tube. The basic principle of operation of the TRANC is the thermal and catalytic conversion of all ΣN_r compounds (including also particulate compounds) to nitric oxide (NO), which is led through PTFE tubing after leaving the TRANC and is analyzed in the CLD at a sampling frequency of 10 Hz. A critical orifice

ensured pressure reduction at a constant flow rate of 1.9 l min^{-1}. Marx et al. (2012), who investigated the field applicability and the conversion efficiency in the laboratory as well as in a long-term field test, found recovery rates for NO_2, NH_3, and a compound mixture (NO_2 and NH_3) of 99%, 95%, and 97%, respectively, in the laboratory, and in the field during an 11-months campaign on average for NO_2 a recovery rate of 91%. Further details of TRANC field applications can be found in Ammann et al. (2012) and Brümmer et al. (2013). A 3-D ultrasonic anemometer (model R3, Gill Instruments, Lymington, UK), measuring the three wind components *u*, *v*, and *w* (which were also used to calculate wind speed (ws), wind direction (wd), and friction velocity (u_*)), was installed at an additional boom next to the TRANC, 30 m above ground. The infrared gas analyzer (IRGA; LI-7500, LI-COR Inc., Lincoln, NE, US) for CO_2 and water vapour (H_2O) was mounted nearby the TRANC on the same boom.

Additionally, air temperature and relative humidity probes (Campbell Scientific, HC2S3, Logan, Utah, USA) were mounted on four levels (10, 20, 40, and 50 m), using the mean of 20 and 40 m for the further analysis. Three leaf wetness sensors (Decagon, LWS, Pullman, Washington, USA) were attached to a spruce tree close to the tower at three different heights (2.1 m: LeafWet_F1, 4.6 m: LeafWet_F2, 6.9 m: LeafWet_F3).

Half-hourly NO and NO_2 (NO_x) data, measured at 50 m height with a chemiluminescence detector (APNA – 360, HORIBA, Tokyo, Japan), as well as precipitation and global radiation data were provided by the Bavarian Forest National Park (Beudert and Breit, 2008, 2010).

For a better speciation of the ΣN_r, a DELTA-Denuder (DEnuder for Long-Term Atmospheric sampling, e.g. Sutton et al., 2001) system was mounted at 30 m height. The system provides monthly NH_3, HNO_3 as well as particulate NO_3^- and particulate NH_4^+ concentrations.

2.3. Data acquisition and flux calculation

The EddyMeas software (part of the software package EddySoft, Kolle and Rebmann, 2009) was used to record all the flux related data: the CLD's and IRGA's analog signals, which were fed into the ultrasonic anemometer interface, as well as the anemometer data itself. The half-hourly exchange fluxes were calculated using the software EddyPro (LI-COR Inc.), which conducted block averaging and 2-D coordinate rotation for ΣN_r and CO_2 fluxes, as well as an application of the WPL term to account for the influence of water vapour on air density fluctuations (Webb et al., 1980) for the latter.

Due to the distance between the inlet and the concentration analyzer, a time lag between the sonic data and the concentration data exists. This time lag can be calculated using the tube length, diameter, and flow rate and was estimated to be approximately 20 s for the TRANC-CLD setup. Another method is to determine the time lag by shifting the time series against each other to maximize the covariance. The shift that is necessary for the maximum (absolute) covariance is assumed to be the time lag under ideal meteorological conditions. In this study, this shift was in a range of 18–21 s, which was set for the ΣN_r concentration time lag span in the EddyPro software package. The software calculates the covariance maximization and also choses the time lag in between the set range. For CO_2 concentrations, measured by an open-path instrument, usually, no or only small time lags (< 1.5 s) occur due to sensor separation. Time lags were estimated by EddyPro's covariance maximization algorithm.

To estimate and correct flux-losses in the high-frequency range, an empirical approach was applied to the ΣN_r fluxes (after Aubinet et al., 2001; Ammann, 1998). The approach is based on the principle of scalar similarity between the cospectrum of vertical wind speed (*w*) and sonic temperature (*T*) cospectra Co(*w*'*T*') with the cospectrum of *w* and ΣN_r concentration Co(*w*'ΣN_r'), where Co(*w*'*T*') is the reference cospectrum. A cospectral damping factor was quantified by fitting spectral transfer functions to the measured (undamped) Co(*w*'*T*') and is followed by a consecutive scaling of Co(*w*'*T*'), multiplied with the obtained transfer function, to the measured Co(*w*'ΣN_r'). The scaling factor is then the damping factor. Because cospectra of every half-hour flux are often noisy due to a wide range of eddy sizes (Kaimal and Finnigan, 1994) and, especially over forest, due to varying surface roughness lengths, the damping factor was calculated monthly for several classes of wind speed and stability. Therefore, the damping factor is subject to significant uncertainty. Resulting damping factors for ΣN_r fluxes separated in four wind sectors and three stability classes (stable, neutral, and unstable) were in the range of 0.65–0.79. Because of the high variability, the overall mean of 0.73 was applied to all ΣN_r fluxes, i.e., measured (damped) fluxes were corrected by dividing them by 0.73. To account for spectral damping in the CO_2 fluxes, the common method of Moncrieff et al. (1997) was used.

In recent campaigns, the same NO analyzer (CLD) was found to be sensitive to ambient water vapour (0.19% sensitivity reduction per 1 mmol mol^{-1} water vapour increase), thereby affecting measured ΣN_r concentrations and, consequently, fluxes. Thus, a correction flux had to be added to every half-hourly ΣN_r flux value, for more details see Ammann et al. (2012) and Brümmer et al. (2013). Correction values ranged from -2 to 0.7 ng N m^{-2} s^{-1} with a mean of -0.3 ng N m^{-2} s^{-1}. In general: negative values indicate deposition and positive values indicate emission fluxes by convention.

Since the IRGA for the CO_2 measurements is an open-path analyzer, periods of rain were excluded from the analysis.

2.4. Data selection and post processing

For the analysis, a time period of 79 days from 14 July to 30 September 2016 (DoY 196–274) was chosen. Before and after this period, a lot of gaps occurred because one of the crucial instruments (IRGA, TRANC, or CLD) was not working properly and had to be maintained or repaired. The half-hourly fluxes of ΣN_r were filtered for low quality (flag = 2, after Mauder and Foken, 2006) and for insufficient turbulence ($u_* < 0.1$ m s^{-1}, see below reasons for this specific number) during the nighttime ($R_g < 5$ W m^{-2}). Additionally, half-hours with higher ΣN_r fluxes than 300 ng N m^{-2} s^{-1} and for half-hourly CO_2, fluxes outside a range of -50 µmol m^{-2} s^{-1} to 30 µmol m^{-2} s^{-1} were removed during daytime and -25 µmol m^{-2} s^{-1} to 30 µmol m^{-2} s^{-1} during nighttime. Only non-gapfilled data were used. The mean random flux errors after Finkelstein and Sims (2001) were 6.0 ng N m^{-2} s^{-1} and 2.6 µmol m^{-2} s^{-1} for ΣN_r and CO_2, respectively (see also Fig. S3). According to Langford et al. (2015), the limits of detection were (1.96 times the flux error, with a confidence limit of 95%) 11.8 ng N m^{-2} s^{-1} and 5.1 µmol m^{-2} s^{-1}. To reduce the random noise in the ΣN_r fluxes, the half-hourly fluxes were averaged to three-hourly means in time steps starting at 01:30 (representing the measurement period from 00:00 until 03:00) until 22:30.

For comparability, the CO_2 fluxes were treated in the same manner except for the u_* threshold. The u_* threshold was calculated using the REddyProc online tool (Wutzler et al., 2018), based on the threshold selection by Papale et al. (2006) and was set to 0.29 m s^{-1}. For ΣN_r, a lower, general u_* threshold of 0.10 m s^{-1} was chosen, as a compromise between no filter and the 0.29 threshold for CO_2, to have at least a minimal filter (as used e.g. in Papale et al. (2006) as a minimum threshold for forest canopies), because at the moment there are no common methods for its evaluation. It has not been investigated until now whether or not ΣN_r (and also other fluxes) should be treated in the same manner as CO_2 and should be the subject of future research. Comparing the ΣN_r fluxes of this study with and without the filter of 0.10 m s^{-1} does not show significant differences for the majority of nights (not shown).

The dataset used in this analysis consisted of 596 three-hourly means for ΣN_r fluxes and of 437 three-hourly means for CO_2 fluxes (out of the 632 possible time steps). Since the driver analysis with artificial neural networks required complete driver and flux data, the number of data points was reduced to 411, as this was the set intersection of all

valid three-hourly means.

The ANNs are programmed in C++ using the CERN-ROOT libraries (Brun and Rademakers, 1997). For all other calculations and figures the statistical programming language R (R Core Team, 2018) was used.

2.5. Artificial neural networks

The inductive methodology presented in Moffat et al. (2010) was used to characterize the ΣN_r and CO_2 fluxes with respect to their biophysical drivers. The methodology is based on artificial neural networks (ANNs) trained with the backpropagation algorithm (Rumelhart et al., 1986; Rojas, 1996). Backpropagation ANNs correspond to statistical multivariate non-linear regressions. During the training, the relationships of the fluxes with the drivers are extracted directly from the data and mapped into the network.

For the driver analysis, the ANN trainings were performed with one input driver at a time to find the most dominant driver. In a second step, the identified primary driver plus one additional driver at a time were fed into the procedure to determine the second most important driver of the fluxes. Each of the ANN trainings was repeated five times to get a measure of the robustness.

Since the trained network is a mathematical representation of ecosystem response to the biophysical drivers, the ANNs can also be used to identify the functional relationships, which can be retrieved in form of equations as it is shown for a single driving variable in Fig. 5, Chapter 3.2.

3. Results and discussion

3.1. Diurnal and seasonal patterns of total reactive nitrogen and carbon dioxide exchange

In Fig. 1, the 79 day period of non-gapfilled ΣN_r and CO_2 fluxes is shown. At this natural forest site, we observe mainly deposition of ΣN_r, with a few exceptions (i.e., emission periods, which cannot be attributed to specific conditions, except comparably low global radiation, see Fig. S2). The three-hourly fluxes were in a range of -127 to 72 ng N m^{-2} s^{-1} with a median of -14 ng N m^{-2} s^{-1} and a mean of -19 ng N m^{-2} s^{-1}. On a half-hourly basis they ranged between -250 and 300 ng N m^{-2} s^{-1} (median -14 ng N m^{-2} s^{-1} and mean of -21 ng N m^{-2} s^{-1}). Comparing these ranges to other studies is difficult due to the fact that most studies only measure one or only selected components of ΣN_r. Hansen et al. (2015) measured NH_3 fluxes in a range of -60 to 120 ng N m^{-2} s^{-1} over a mixed forest but with a lot more emission phases with a focus on post-leaf fall periods. NH_3 was on average 33% of ΣN_r and is next to NO_2 (i.e. Horii et al., 2004) the main component, which undergoes bi-directional exchange even in natural ecosystems. Therefore, it was expectable that we measured higher deposition rates due to most of the other ΣN_r components, which are usually deposited. One exception might be NO, but this component has only a very small share above such a natural forest site (see Fig. S2) and is commonly observed as soil efflux when produced as byproduct of nitrification or as an intermediate product of denitrification (Butterbach-Bahl et al., 1997; Rosenkranz et al., 2006). Horii et al. (2006) measured only deposition fluxes for all oxidized atmospheric nitrogen species (NO_y), up to approx. -80 ng N m^{-2} s^{-1}, also above a mixed forest. Similar findings were reported by Munger et al. (1996) for the same site. In contrast, Horii et al. (2004) showed NO_2 emission fluxes, small NO deposition fluxes, and HNO_3 deposition fluxes almost as high as the NO_y fluxes (Horii et al., 2006), which shows that HNO_3 appears to be a great share to the ΣN_r deposition even though the concentrations are comparably low. Furthermore, Munger et al. (1996) state that HNO_3 formation is an effective pathway to remove NO_x by the reaction of NO_2 and O_3. These findings emphasize how difficult interpretations of mixed flux signals are. There is not only the daily conversion between NO and NO_2, but also the reaction to other NO_y compounds. Additionally, all ΣN_r components underlie differently directed exchange, take different pathways, and differ in their exchange velocities.

There are only very few studies which measure the sum of all reactive nitrogen compounds exchange. In one study featuring the same ΣN_r measurement setup (Brümmer et al., 2013) above agricultural land, half-hourly fluxes in the range from -175 up to more than 4000 ng N m^{-2} s^{-1} were observed, the latter induced by a fertilization event. More distant to that event their fluxes ranged mainly between –20 and 20 ng N m^{-2} s^{-1}. As an unmanaged forest, our site was obviously able to take up more ΣN_r, but still in the same order of magnitude. It also seems as if the arable site exhibited mostly neutral exchange outside of management events, in contrast to our forest site which appears to be a sink. This may be explained by the higher amount of bi-directionally exchanged NH_3 and very high short-term nitrogen concentrations in agricultural environments.

Generally, a diurnal cycle with consistently low negative or neutral ΣN_r fluxes during the night, increasing deposition during the morning hours and decreasing deposition in the evening was observed (Fig. 2).

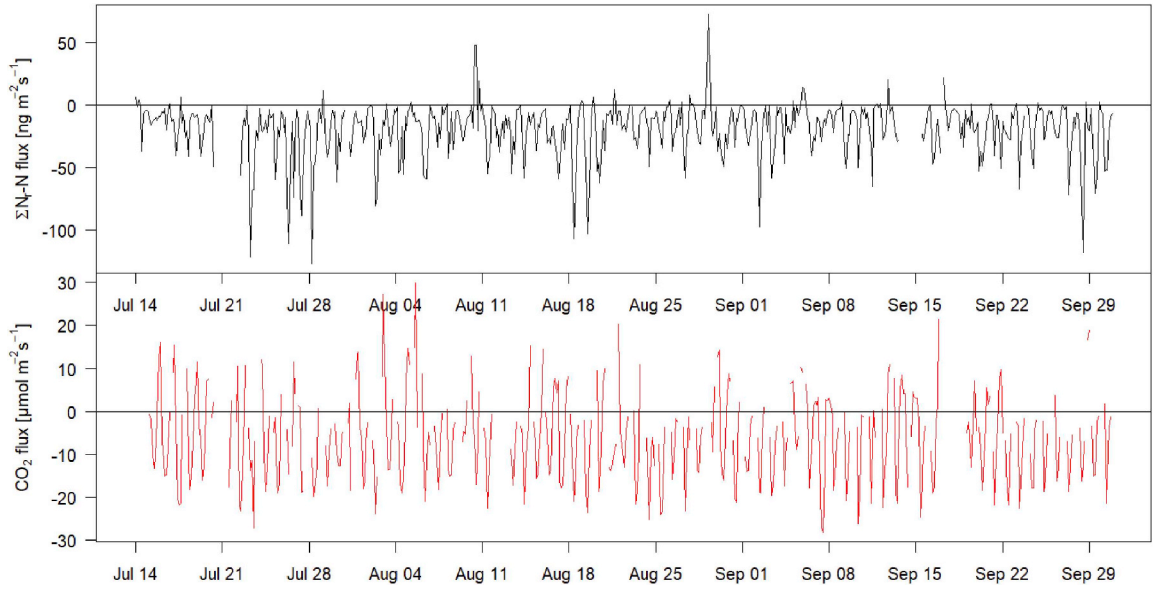

Fig. 1. Non-gapfilled time series of 3-h-mean total reactive nitrogen (black) and carbon dioxide (red) fluxes.

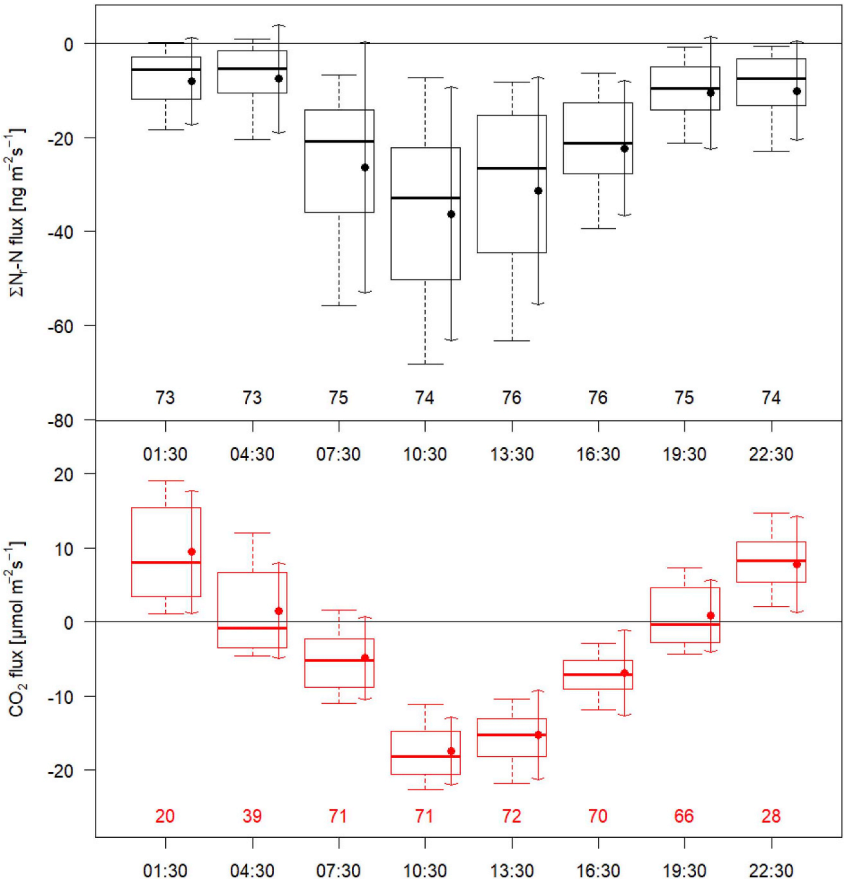

Fig. 2. Diurnal cycles of 3-h-mean total reactive nitrogen (black) and carbon dioxide (red) fluxes, depicted as boxplots (whiskers = 1st and 9th deciles, box frame = quartiles, bold line = median) plus mean values (dots right of the boxplot center) and standard deviation (arrows). The numbers below represent the *n* of the respective group, possible maximum is 79.

Wyers and Erisman (1998) observed NH_3 fluxes above coniferous forest with very similar diurnal cycles, as well as Geddes and Murphy (2014) and Horii et al. (2006) for summer NO_y fluxes above mixed forests. Similar observations were made by Wolff et al. (2010) for total ammonium and total nitrate above spruce canopy.

Three-hourly CO_2 fluxes varied between -28 and 30 µmol m^{-2} s^{-1} with a median and mean of -6 µmol m^{-2} s^{-1}. On a half-hourly basis they ranged between -40 and 30 µmol m^{-2} s^{-1}, with a median and mean of -9 µmol m^{-2} s^{-1}. The diurnal pattern for CO_2 is typical for exchange during the vegetation period in a temperate coniferous forest (e.g. Falge et al., 2002; Chen et al., 2009). In the night, CO_2 release was observed, i.e. ecosystem respiration is the main component of net ecosystem exchange while no photosynthesis occurs. Mean respiration fluxes of 9 µmol m^{-2} s^{-1} were observed. During the day, CO_2 uptake up to 17 µmol m^{-2} s^{-1} was observed when photosynthesis dominates over ecosystem respiration. These ranges are in agreement with the mean values for July, August and September (1996–2000) for the Tharandt forest, also mainly consisting of spruce species (Falge et al., 2002).

3.2. Artificial neural network analysis

To characterize the importance of biophysical drivers of ΣN_r and CO_2 exchange, an ANN analysis was conducted. ANNs depict the correlation between the input variables and the output, here the fluxes. In the first step, the fluxes were mapped with one single variable at a time (upper part of Figs. 3 and 4). The goodness-of-fit is expressed as R^2 on the *y*-axis and given for a set of variables on the *x*-axis (see Table S1 for abbreviations and Fig. S4 for time series). The R^2 values for CO_2 exchange are distinctively higher than for ΣN_r, because the ecosystem-physiological processes of CO_2 are mainly driven by the meteorology. Meanwhile, the processes for ΣN_r are not as obvious and other drivers (that have not or cannot be measured), combined or opposing effects of subcomponents (like NO_x or NH_3), and lagged or higher-temporal-scale effects lead to lower R^2 values.

Highest R^2 for ΣN_r fluxes were reached with ΣN_r concentration ($R^2 = 0.24$), global radiation ($R^2 = 0.22$), and for the correlation with CO_2 flux ($R^2 = 0.17$) as a primary driver. The question remains whether the concentration is a driver of the flux or vice versa, as previously discussed in Zöll et al. (2016) or Milford (2004). During deposition situations, it is assumed that higher concentrations lead to higher deposition due to a larger concentration difference between the measurement height and the surface. We measured in a N limited natural ecosystem and therefore mainly observed deposition, the reverse case of fluxes controlling the concentrations seems highly unlikely even during the few emission phases. Though fluxes always lead to a change of the regarded volume, and hence also the concentration regime, in this study the concentration might be the controlling variable. The dominant biophysical control was global radiation, which is known to highly influence the opening of stomata (Jarvis, 1976). This is a major pathway for CO_2 exchange, but also for other compounds such as NH_3 (Wyers and Erisman, 1998; Hansen et al., 2015) and NO_2 (Thoene et al., 1996), which are – depending on site location – usually the main components of ΣN_r (Marx et al., 2012).

In the second step, the dominant climatic driver global radiation, was chosen as primary driver. It was then tested to which extent the flux can be explained by global radiation plus another parameter (Fig. 3). Then the R^2 with ΣN_r concentration as secondary driver becomes as high as 0.41, and the combined amount is slightly lower than adding the R^2 of both primary drivers. This means that both drivers (global radiation and ΣN_r concentration) add independent information to explain the variability in the ΣN_r fluxes. On the contrary, adding CO_2 as a second driver increases R^2 only slightly and indicates that most of the information is already contained in global radiation. This can be expected since global radiation is also the main driver of CO_2 fluxes. In addition, one would expect the humidity variables to stand out, too, like it was observed by Milford et al. (2001) for NH_3 above moorland.

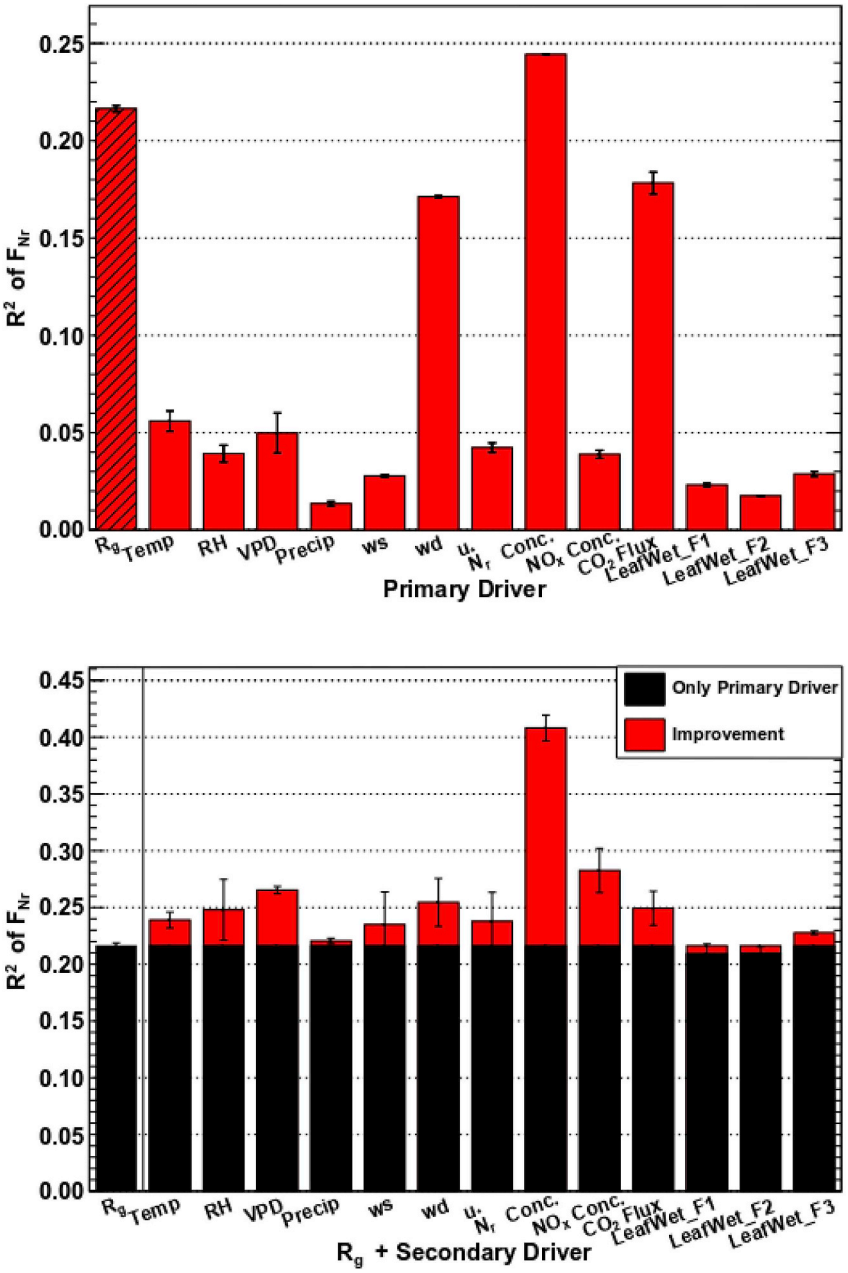

Fig. 3. Primary (upper panel) and secondary (lower panel) driver analysis by the artificial neural networks for 3-h-mean total reactive nitrogen fluxes, only for selected drivers. As primary driver global radiation was chosen.

Surface wetness is a perfect sink for NH_3 due to its high solubility (Wentworth et al., 2016). However, we only measured NH_3 as a part of ΣN_r, and humidity generally plays a bigger role in ecosystems like peatlands (as in Milford et al., 2001), hence the effect at our site was probably minor compared to the others. After all, vapour pressure deficit (VPD) increases R^2 by 5% as a secondary driver.

For CO_2 fluxes, global radiation as a primary driver yields the highest R^2 of 0.66. This means that as expected the radiative driver is the most important driver of the CO_2 fluxes which is in agreement to other studies using ANNs to explain CO_2 fluxes (Moffat et al., 2010; Park et al., 2018). The correlation of the two fluxes, CO_2 and ΣN_r, is the same as above (R^2 = 0.17). For CO_2 fluxes, no parameter increases R^2 considerably as secondary driver to the global radiation. The CO_2 fluxes of this natural, unstressed forest during this summer period were mainly dominated by the photosynthesis response during daytime with little influence of the other drivers like temperature or humidity, since we captured no drought or heat nor very cold periods suppressing photosynthesis.

The ΣN_r and CO_2 fluxes have both shown a similar diurnal cycle and a strong response to global radiation as a driver. Only slightly increasing R^2 as a secondary variable tells us that their main linkage is through global radiation. It is not surprising that this parameter plays an important role, since it is the main driver for opening the stomata, which is an important pathway for both exchange fluxes or at least partly for some ΣN_r compounds (especially NH_3 and NO_2).

To investigate this further, the ANNs were also used to determine the light response curves for both fluxes (Fig. 5).

In Fig. 5, the light response curves for ΣN_r (upper panel) and CO_2 flux (lower panel) are shown. For CO_2, the typical light saturation curve can be observed (i.e. Milford et al., 2001, Krishnan et al., 2009; Moffat et al., 2010): starting with a linear decrease during nighttime and saturating towards high global radiation. In contrast, the ΣN_r flux light

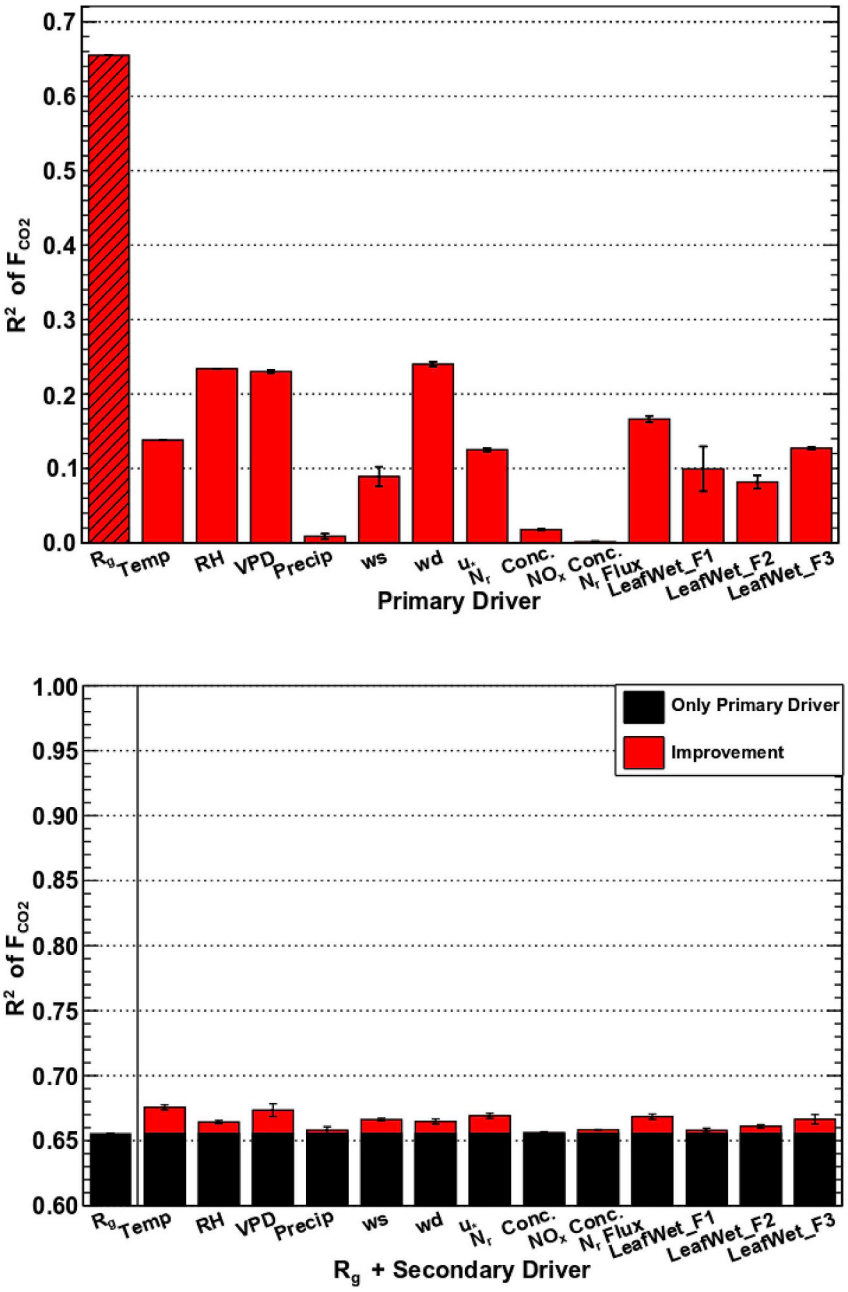

Fig. 4. Primary (upper panel) and secondary (lower panel) driver analysis by the artificial neural networks for 3-h-mean carbon dioxide fluxes, only for selected drivers. As primary driver global radiation was chosen.

response curve is slightly bell-shaped: starting with a decrease during nighttime, reaching a minimum around 600 $W m^{-2}$, and then increasing again for higher radiation values. Hence, the ΣN_r exchange reaches a reversal point rather than a threshold of saturation as for CO_2 with increasing light. The question remains if this is specific for our site, the year, the time of the year, the land use, or only for certain nitrogen compounds. In contrary to CO_2, the ΣN_r compounds are not as actively consumed by the plant. Usually it is assumed that the stomatal compensation point (Farquhar et al., 1980) regulates the amount of uptake. The concept of a compensation point originates from NH_3 exchange and is based on the idea that the flux is driven by the difference between ambient concentrations and a nonzero air NH_3 concentration in equilibrium with the apoplastic fluid. Besides, compensation points are also evaluated for NO_2 (Thoene et al., 1996). This means we observe deposition as long as the stomatal concentration is lower than the outside concentration and the stronger this gradient the more deposition or uptake occurs. So at some point not the opening of the stomata itself influences the uptake but the compensation point which is mainly regulated by the surrounding concentration, which is limited at our remote site. This matches also our former findings, that the ΣN_r concentration is an important driver for the ΣN_r exchange. It has to be noted that u_* did not emerge as a strong driver for ΣN_r deposition. The higher dependence on radiation suggests that photochemistry, which drives the speciation of ΣN_r, might be more important than turbulence alone. Higher radiation leads to more photochemical reactions through which O_3 is formed. This might affect the ΣN_r composition and therefore the exchange characteristic of ΣN_r. Eventually, more HNO_3, characterized by high deposition velocities (Horii et al., 2004), is formed because of enhanced reaction of NO_2 and O_3 (Munger et al., 1996), which leads to higher ΣN_r deposition during the day.

There are some studies mostly driven by the hypothesis, that increasing reactive nitrogen deposition leads to a fertilization effect on

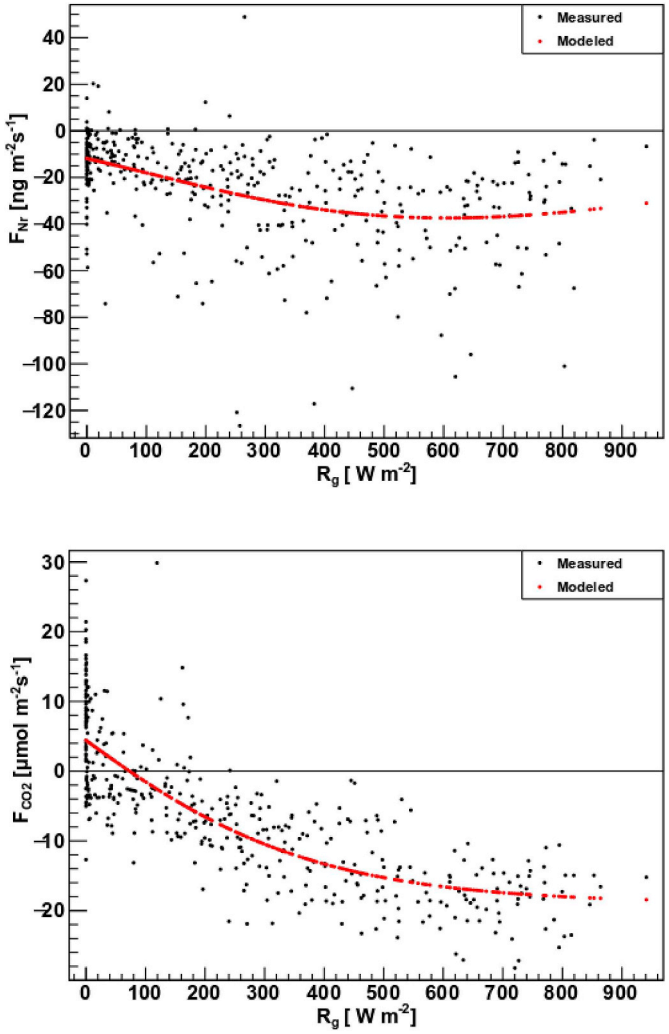

Fig. 5. Light response of 3-h –mean total reactive nitrogen fluxes (upper panel) and carbon dioxide fluxes (lower panel), evaluated by the artificial neural networks.

natural, unmanaged ecosystems, which then increase their biomass and therefore act as a potentially higher sink for carbon (Field et al., 2017). Meanwhile, some studies could show that soil C storage increases with increasing reactive nitrogen deposition (e.g. Field et al., 2017; Maaroufi et al., 2015) and that photosynthetic capacity increases up to a certain extent (evergreen forests, Fleischer et al., 2013; meadow, Song et al., 2017). However, these were all studies on long-term effects. The data basis on short-term effects is even smaller. Milford et al. (2001) showed that NH_3 exchange was mainly driven by ambient concentrations, wetness as well as canopy temperature, even though they stated that the exchange is usually also to some extent dependent on radiation because the stomatal pathway appeared to be important. This was likewise the case at our site for the sum of all reactive nitrogen compounds (Fig. 3). Fleischer et al. (2013) could not rule out that the increase in photosynthetic capacity was at least partly induced by the change in climatic conditions due to global change. Our finding that the concentration is a major driver of the ΣN_r fluxes strongly supports their hypothesis that the increase of photosynthetic capacity is induced by the increase in reactive nitrogen deposition. The other dominant driver global radiation will be only little affected by global climate change. However, there might be further indirect effects by temperature increase through the availability of ΣN_r, which might be increased due to elevated reactive nitrogen emissions (Sutton et al., 2013).

3.3. Residual flux and additional biophysical controls analysis

For further analysis of ΣN_r relationships the residual fluxes of the light response curve modelled by the ANNs were used. These residual fluxes are here defined as the difference between the measured value and the modelled light response for each 3-h mean flux. The closer the measured value is to the modelled value, the smaller is the residual flux. Negative or positive residual fluxes do not indicate whether the flux is a deposition or an emission flux, but a negative residual value indicates stronger deposition induced by the secondary driver than predicted by the light response curve (as a proxy for the diurnal cycle) alone.

Analysing residual fluxes instead of directly measured fluxes ensures that the influence of the interrelation between other possible drivers with distinct diurnal variability like, e.g., global radiation and temperature is removed.

The diurnal cycle of the residual fluxes exhibited no distinct variability, especially not for the CO_2 fluxes (Fig. 6). Means and medians stayed around zero. Therefore, we can exclude that any other variable than global radiation had a significant influence on the diurnal variability. For ΣN_r, the residual fluxes had a larger range during the day than during the night. At 6:00 to 9:00 and 9:00 to 12:00 mean values tended to be negative, while the other 3 h values are shifted towards positive ΣN_r flux residuals.

However, even though the mean and median global radiation situation is comparable for both time frames, 10:30 and 13:30 (see Fig. S3), highest ΣN_r deposition and CO_2 uptake can be observed at 10:30 (Fig. 2). Other variables than radiation seem to cause this behavior since the median and mean residual fluxes are shifted towards positive or less negative residual fluxes at 13:30 (Fig. 6). A well-mixed atmosphere at around 13:30 seems to be less efficient for the deposition or uptake by plants than probable occurring gradients earlier during the day as also suggested by the highest residual ΣN_r deposition fluxes occurring at 7:30 (Fig. 6).

Residual fluxes stratified by different classes of meteorological conditions, ΣN_r concentrations, and surface wetness (Fig. 7) show some clear patterns under given conditions. For example, residual fluxes, which occurred during higher concentration conditions (> 4.5 ppb, 4.5 ppb is the overall median) tended to be neutral or negative. Higher deposition occurred during the day (Fig. 7a). The finding of increasing deposition with increasing concentrations has been reported earlier, e.g., for ΣN_r by Brümmer et al. (2013), and for NH_3 by Zöll et al. (2016). Further, high temperatures favored high residual uptake fluxes during the morning hours. Higher temperatures (> 15 °C) also lead to increased plant activity enhancing deposition, which was also observed by Wolff et al. (2010) for total nitrate and total ammonium fluxes. Further aerosols might be less stable at higher temperatures, converting to e.g. ammonia with higher deposition velocities. Typically high residual emission fluxes of around 7 ng N m^{-2} s^{-1} were also found during daytime under low VPD. So less uptake or even emission occurred. Dry leaves supported very high residual uptake fluxes of 13 ng N m^{-2} s^{-1}, especially in the morning hours. Generally it was observed, that during precipitation (not shown) or wet conditions (Fig. 7c) low deposition or emission fluxes occur, in contrast to observations of Wyers and Erisman (1998) who recorded maximum NH_3 depositions when the canopy was wet, i.e. under high canopy water storage conditions (CWS > 2 mm). But Wolff et al. (2010) also observed higher deposition of total nitrate and total ammonium during dry conditions (no rain, low RH). Regarding the concentrations stratified by wet and dry leafs (not shown) slightly higher concentrations occur during dry conditions, which is an indicator for efficient wet deposition that removes most of the ΣN_r before reaching the site during rainy periods. Then Fig. 7 emphasizes again that nitrogen concentration plays a major role for the exchange, as it was already shown by the ANNs, even at a natural, remote site, so that elevated concentrations lead to higher deposition under the favorable conditions like higher temperatures, higher VPD, and dry leaf surfaces. Taking flux errors into account (Fig. S5), reveals that residual

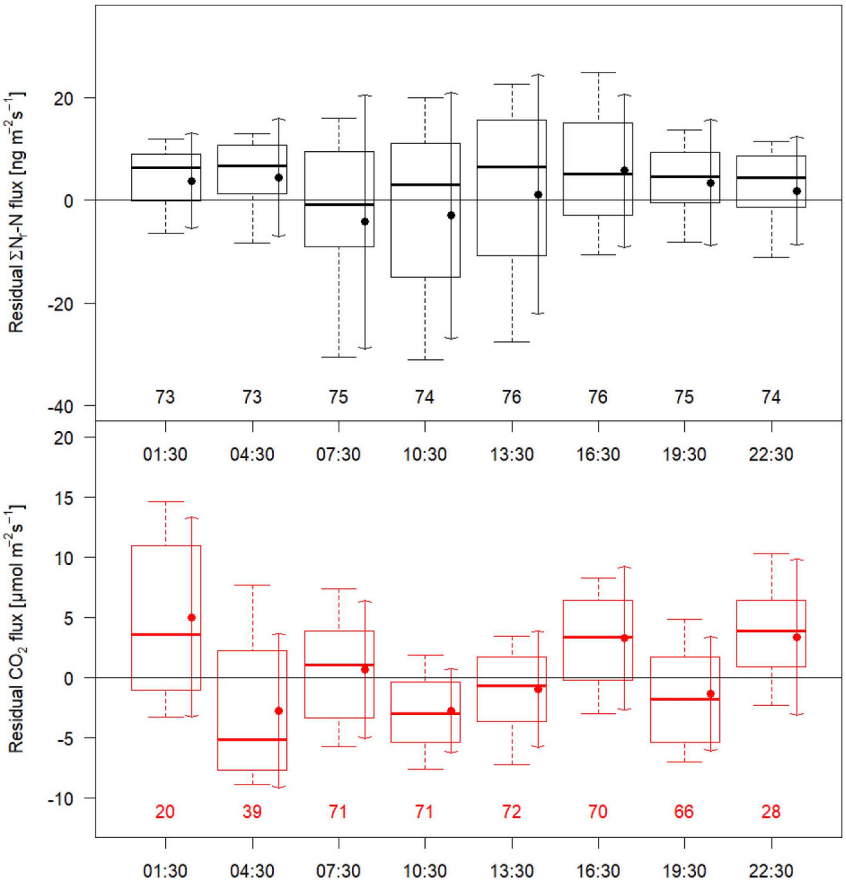

Fig. 6. Diurnal cycles of 3-h-mean residual total reactive nitrogen (black) and carbon dioxide (red) fluxes, depicted as boxplots (whiskers = 1st and 9th deciles, box frame = quartiles, bold line = median) plus mean values (dots right of the boxplot center) and standard deviation (arrows). The numbers below represent the *n* of the respective group, possible maximum is 79.

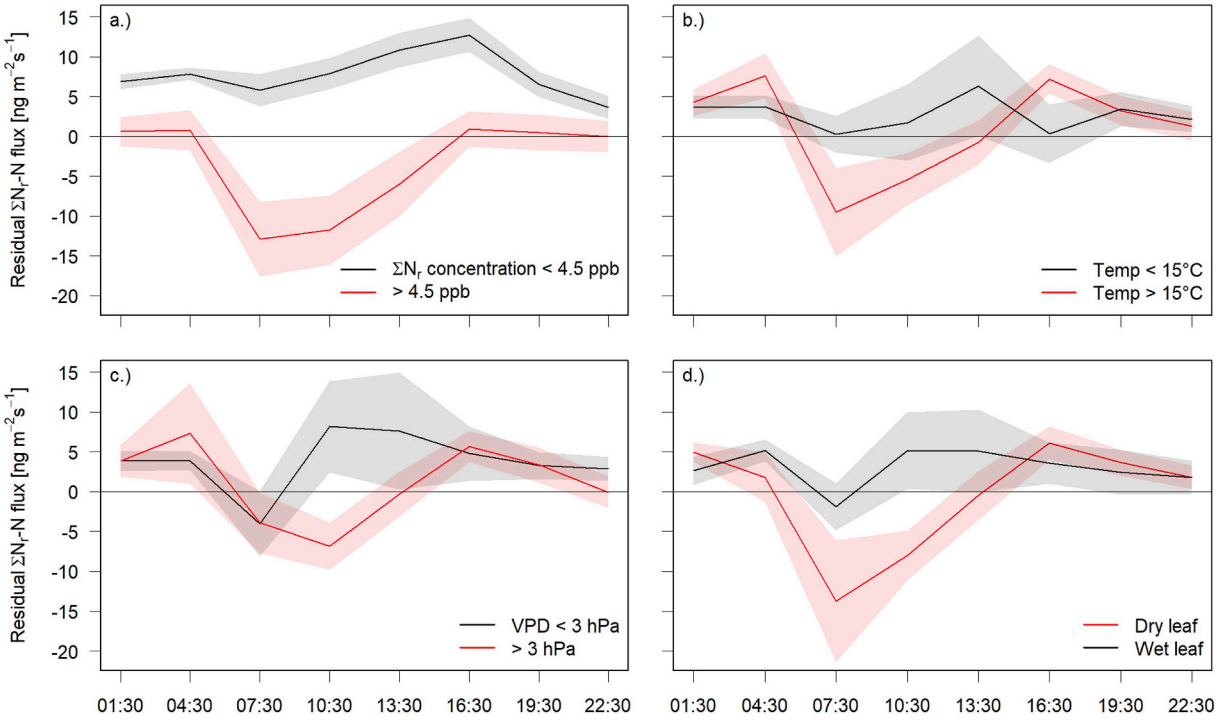

Fig. 7. Mean diurnal variation of residual total reactive nitrogen fluxes (3-h-mean) separated by concentration (a.) air temperature (b.), VPD (c.) and leaf wetness (d.). Shaded areas represent standard errors of the mean.

fluxes were sometimes smaller than the error. Therefore the tendencies observed during the day might be treated with even more caution. Additionally, mean diurnal concentration normalized ΣN_r fluxes can be found in the supplement (Fig. S6). Those quasi deposition velocities provided no further insights since ΣN_r includes several compounds with very different exchange behaviors and interactions and reactions between them, which makes it impossible to provide one deposition velocity for all of them. Therefore, a concentration dependence is still existent (Fig. S6a).

4. Conclusion

Background ΣN_r fluxes and CO_2 fluxes were characterized from July to September above a mixed forest in the Bavarian Forest National Park. The diurnal cycles of the ΣN_r exchange were similar compared to other studies (about one or several ΣN_r compounds), showing mainly deposition with higher deposition rates during the day. An almost identical pattern was observed for the measured CO_2 exchange, except for the fact that CO_2 is being released during night, whereas the mean ΣN_r flux approaches almost zero but stays negative. Applying the method of artificial neural networks, two dominant drivers for ΣN_r exchange could be detected: the concentration of ΣN_r itself and global radiation. The latter is also the main driver for CO_2 exchange and therefore the main linkage between ΣN_r and CO_2 exchange found in this study. Further interrelations of ΣN_r flux are complex and could only be analyzed by data stratification and residual flux analysis. It becomes apparent that fluxes tend to become less negative – less deposition occurs – during wet and cooler conditions, which is an indicator for efficient wet deposition that removes most of the atmospheric ΣN_r before reaching the site.

Future modelling studies can benefit from our observations that there is a linkage between ΣN_r and CO_2 exchange via radiation as it was already suggested by Farquhar et al. (1980) in the context of a stomatal compensation point. Further research needs to be done for several ΣN_r concentration levels, different land uses, and possibly also for separate nitrogen compounds.

5. Data availability

Data will be archived and are available from the corresponding author on request.

Declaration of interests

The authors declare that they have no known competing financial interests or personal relationships that could have appeared to influence the work reported in this paper.

Acknowledgements

Funding for this study from the German Environment Agency under the guidance of Dr. Markus Geupel (project FORESTFLUX, support code FKZ 3715512110) and from the German Federal Ministry of Education and Research (BMBF) within the framework of the Junior Research Group NITROSPHERE under support code FKZ 01LN1308A is greatly acknowledged. We thank Jeremy Rüffer and Jean-Pierre Delorme for excellent technical support as well as Ute Tambor, Andrea Niemeyer, and Dr. Daniel Ziehe for conducting laboratory analyses of denuder and filter samples. Christ of Ammann is thanked for his scientific advice. We further like to thank the Bavarian Forest National Park Administration for outstanding site support by Wilhelm Breit and Ludwig Höcker.

Appendix A. Supplementary data

Supplementary data to this article can be found online at https://doi.org/10.1016/j.atmosenv.2019.02.042.

References

Albert, L.P., Keenan, T.F., Burns, S.P., Huxman, T.E., Monson, R.K., 2017. Climate controls over ecosystem metabolism: insights from a fifteen-year inductive artificial neural network synthesis for a subalpine forest. Oecologia 184, 25–41.

Ammann, C., 1998. On the Applicability of Relaxed Eddy Accumulation and Common Methods for Measuring Trace Gas Surface Fluxes. PhD Thesis. Swiss Federal Institute of Technology, Zurich, Switzerland, pp. 229.

Ammann, C., Wolff, V., Marx, O., Brümmer, C., Neftel, A., 2012. Measuring the biosphere-atmosphere exchange of total reactive nitrogen by eddy covariance. Biogeosciences 9, 4247–4261. https://doi.org/10.5194/bg-9-4247-2012.

Aubinet, M., Grelle, A., Ibrom, A., Rannik, U., Moncrieff, J., Foken, T., Kowalski, A.S., Martin, P.H., Berbigier, P., Bernhofer, Ch., Clement, R., Elbers, J., Granier, A., Grünwald, T., Morgenstern, K., Pilegaard, K., Rebmann, C., Snijders, W., Valentini, R., Vesala, T., 2001. Estimates of the annual net carbon and water exchange of forests: the EUROFLUX methodology. Adv. Ecol. Res. 30, 113–171.

Beudert, B., Breit, W., 2008. Integrated Monitoring Programm an der Meßstelle Forellenbach im Nationalpark Bayerischer Wald, Untersuchungen zu Prozessen und Räumen der Hochwasserbildung im Forellenbachgebiet, Förderkennzeichen 351 01 012, Nationalparkverwaltung Bayerischer Wald. Sachgebiet IV. docplayer.org/80741933-Integrated-monitoring-programm-an-der-messstelle-forellenbach-im-nationalpark-bayerischer-wald.html, Accessed date: 6 August 2018.

Beudert, B., Breit, W., 2010. Integrated Monitoring Programm an der Meßstelle Forellenbach im Nationalpark Bayerischer Wald, Untersuchungen zum Stickstoffeintrag und zum wassergebundenen Stickstoffhaushalt des Forellenbachgebiets, Förderkennzeichen 351 01 012. Nationalparkverwaltung Bayerischer Wald, Sachgebiet IV. www.umweltbundesamt.de/sites/default/files/medien/370/dokumente/ece_im_forellenbach_berichtsjahr_2009.pdf, Accessed date: 6 August 2018.

Beudert, B., Bässler, C., Thorn, S., Noss, R., Schröder, B., Dieffenbach-Fries, H., Foullois, N., Müller, J., 2014. Bark beetles increase biodiversity while maintaining drinking water quality. Conserv. Lett. 8 (4), 272–281.

Beudert, B., Gietl, G., 2015. Long-term monitoring in the Große Ohe catchment, bavarian forest national Park. Silva Gabreta 21 (1), 5–27.

Beudert, B., Bernsteinová, J., Premier, J., Bässler, C., 2018. Natural disturbance by bark beetle offsets climate change effects on streamflow in headwater catchments of the Bohemian Forest. Silva Gabreta 24, 21–45.

Brümmer, C., Marx, O., Kutsch, W., Ammann, C., Wolff, V., Flechard, C.R., Freibauer, A., 2013. Fluxes of total reactive atmospheric nitrogen (ΣN_r) using eddy covariance above arable land. Tellus B 65, 19770.

Brun, R., Rademakers, F., 1997. ROOT - an object oriented data analysis framework. Nucl. Instrum. Methods Phys. Res., Sect. A 389, 81–86. See also. http://root.cern.ch/.

Butterbach-Bahl, K., Gasche, R., Breuer, L., Papen, H., 1997. Fluxes of NO and N_2O from temperate forest soils: impact of forest type, N deposition and of liming on the NO and N_2O emissions. Nutrient Cycl. Agroecosyst. 48, 79–90.

Chen, B., Black, T.A., Coops, N.C., Krishnan, P., Jassal, R., Brümmer, C., Nesic, Z., 2009. Seasonal controls on interannual variability in carbon dioxide exchange of a near--end-of rotation Douglas-fir stand in the Pacific Northwest, 1997–2006. Glob. Chang. Biol. 15, 1962–1981.

Erisman, J.W., Galloway, J.N., Seitzinger, S., Bleeker, A., Dise, N.B., Petrescu, A.M.R., Leach, A.M., de Vries, W., 2013. Consequences of human modification of the global nitrogen cycle. Phil. Trans. Biol. Sci. 368, 20130116.

Falge, E., Tenhunen, J., Baldocchi, D., Aubinet, M., Bakwin, P., Berbigier, P., Bernhofer, C., Bonnefond, J.-M., Burba, G., Clement, R., Davis, K.J., Elbers, J.A., Falk, M., Goldstein, A.H., Grelle, A., Granier, A., Grünwald, T., Gundmondsson, J., Hollinger, D., Janssens, I.A., Keronen, P., Kowalski, A.S., Katul, G., Law, B.E., Malhi, Y., Meyers, T., Monson, R.K., Moors, E., Munger, J.W., Oechel, W., Paw, U.K., Pilegaard, K., Rannik, U., Rebmann, C., Suyker, A.E., Thorgeirsson, H., Tirone, G., Turnipseed, A., Wilson, K., Wofsy, S., 2002. Phase and amplitude of ecosystem carbon release and uptake potentials as derived from FLUXNET measurements. Agric. For. Meteorol. 113, 75–95.

Farquhar, G.D., Firth, P.M., Wetselaar, R., Weir, B., 1980. On the gaseous exchange of ammonia between leaves and the environment: determination of the ammonia compensation point. Plant Physiol. 66, 710–714.

Field, C.D., Evans, C.D., Dise, N.B., Hall, J.R., Caporn, S.J.M., 2017. Long-term nitrogen deposition increases heathland carbon sequestration. Sci. Total Environ. 592, 426–435.

Finkelstein, P.L., Sims, P.F., 2001. Sampling error in eddy correlation flux measurements. J. Geophys. Res. 106, 3503–3509.

Flechard, C.R., Fowler, D., 1998. Atmospheric Ammonia at a Moorland Site. II: Long-Term Surface-Atmosphere Micrometeorological Flux Measurements. Royal Meteorological Society, pp. 759–791.

Flechard, C.R., Massad, R.-S., Loubet, B., Personne, E., Simpson, D., Bash, J.O., Cooter, E.J., Nemitz, E., Sutton, M.A., 2013. Advances in understanding, models and parameterizations of biosphere-atmosphere ammonia exchange. Biogeosciences 10, 5183–5225.

Fleischer, K., Rebel, K.T., van der Molen, M.K., Erisman, J.W., Wassen, M.J., van Loon, E.E., Montagnani, L., Gough, C.M., Herbst, M., Janssens, I.A., Gianelle, D., Dolman, A.J., 2013. The contribution of nitrogen deposition to the photosynthetic capacity of forests. Glob. Biogeochem. Cycles 27, 187–199.

Follett, R.F., Hatfield, J.L., 2001. Nitrogen in the environment: sources, problems, and management. In Optimizing nitrogen management in food and energy production and environmental protection. Sci. World 1 (S2), 920–926 Proceedings of the 2nd International Nitrogen Conference on Science and Policy.

Fowler, D., Coyle, M., Skiba, U., Sutton, M.A., Cape, J.N., Reis, S., Sheppard, L.J., Jenkins,

A., Grizzetti, B., Galloway, J.N., Vitousek, P., Leach, A., Bouwman, A.F., Butterbach-Bahl, K., Dentener, F., Stevenson, D., Amann, M., Voss, M., 2013. The global nitrogen cycle in the twenty-first century. Phil. Trans. Biol. Sci. 368, 20130164. https://doi.org/10.1098/rstb.2013.0164.

Geddes, J.A., Murphy, J.G., 2014. Observations of reactive nitrogen oxide fluxes by eddy covariance above two midlatitude North American mixed hardwood forests. Atmos. Chem. Phys. 14, 2939–2957.

Hansen, K., Pryor, S.C., Boegh, E., Hornsby, K.E., Jensen, B., Sørensen, L.L., 2015. Background concentrations and fluxes of atmospheric ammonia over a deciduous forest. Agric. For. Meteorol. 214–215, 380–392.

Horii, C.V., William Munger, J., Wofsy, S.C., Zahniser, M., Nelson, D., Barry McManus, J., 2004. Fluxes of nitrogen oxides over temperate deciduous forest. J. Geophys. Res. 109, D08305.

Horii, C.V., William Munger, J., Wofsy, S.C., Zahniser, M., Nelson, D., Barry McManus, J., 2006. Atmospheric reactive nitrogen concentration and flux budgets at a Northeastern U.S. forest site. Agric. For. Meteorol. 136, 159–174.

Hurkuck, M., Brümmer, C., Mohr, K., Grünhage, L., Flessa, H., Kutsch, W.L., 2014. Determination of atmospheric nitrogen deposition to a semi-natural peat bog site in an intensively managed agricultural landscape. Atmos. Environ. 97, 296–309.

Jarvis, P.G., 1976. The interpretation of the variations in leaf water potential and stomatal conductance found in canopies in the field. Phil. Trans. Roy. Soc. Lond. B 273, 593–610. https://doi.org/10.1098/rstb.1976.0035.

Kaimal, J., Finnigan, J., 1994. Atmospheric Boundary Layer Flows: Their Structure and Measurement. Oxford University Press, UK, pp. 289.

Kolle, O., Rebmann, C., 2009. EddySoft Documentation of a Software Package to Acquire and Process Eddy Covariance Data. MPI-BGC.

Krishnan, P., Black, T.A., Jassal, R.S., Chen, B., Nesic, Z., 2009. Interannual variability of the carbon balance of three different-aged Douglas-fir stands in the Pacific Northwest. J. Geophys. Res.: Biogeosciences 114.

Langford, B., Acton, W., Ammann, C., Valach, A., Nemitz, E., 2015. Eddy-covariance data with low signal-to-noise ratio: time-lag determination, uncertainties and limit of detection. Atmos. Meas. Technol. 8, 4197–4213.

Maaroufi, N.I., Nordin, A., Hasselquist, N.J., Bach, L.H., Palmqvist, K., Gundale, M.J., 2015. Anthropogenic nitrogen deposition enhances carbon sequestration in boreal soils. Glob. Chang. Biol. 21, 3169–3180.

Marx, O., Brümmer, C., Ammann, C., Wolff, V., Freibauer, A., 2012. TRANC - a novel fast-response converter to measure total reactive atmospheric nitrogen. Atmos. Meas. Technol. 5, 1045–1057.

Mauder, M., Foken, T., 2006. Impact of post-field data processing on eddy covariance flux estimates and energy balance closure. Meteorol. Z. 15, 597–609.

Milford, C., Hargreaves, K.J., Sutton, M.A., Loubet, B., Cellier, P., 2001. Fluxes of NH_3 and CO_2 over upland moorland in the vicinity of agricultural land. J. Geophys. Res. Atmos. 106, 24169–24181.

Milford, C., 2004. Dynamics of Atmospheric Ammonia Exchange with Intensively-Managed Grassland, Doctor of Philosophy. The University of Edinburgh, pp. 218.

Moffat, A.M., Beckstein, C., Churkina, G., Mund, M., Heimann, M., 2010. Characterization of ecosystem responses to climatic controls using artificial neural networks. Glob. Chang. Biol. 16, 2737–2749.

Moncrieff, J.B., Massheder, J.M., de Bruin, H., Elbers, J., Friborg, T., Heusinkveld, B., Kabat, P., Scott, S., Soegaard, H., Verhoef, A., 1997. A system to measure surface fluxes of momentum, sensible heat, water vapour and carbon dioxide. J. Hydrol. 188–189, 589–611.

Munger, J.W., Wofsy, S.C., Bakwin, P.S., Fan, S.-M., Goulden, M.L., Daube, B.C., Goldstein, A.H., 1996. Atmospheric deposition of reactive nitrogen oxides and ozone in a temperate deciduous forest and a subarctic woodland. 1. Measurements and mechanisms. J. Geophys. Res. 101 (NO. D7), 12639–12657.

Papale, D., Reichstein, M., Aubinet, M., Canfora, E., Bernhofer, C., Kutsch, W., Longdoz, B., Rambal, S., Valentini, R., Vesala, T., Yakir, D., 2006. Towards a standardized processing of Net Ecosystem Exchange measured with eddy covariance technique: algorithms and uncertainty estimation. Biogeosciences 3, 571–583.

Park, S.-B., Knohl, A., Lucas-Moffat, A.M., Migliavacca, M., Gerbig, C., Vesala, T., Peltola, O., Mammarella, I., Kolle, O., Lavrič, J.V., Prokushkin, A., Heimann, M., 2018. Strong radiative effect induced by clouds and smoke on forest net ecosystem productivity in central Siberia. Agric. For. Meteorol. 250-251, 376–387.

R Core Team, 2018. R: A Language and Environment for Statistical Computing. R Foundation for Statistical Computing, Vienna, Austria3-900051-07-0. https://www.R-project.org/.

Rojas, R., 1996. Neural Networks - A Systematic Introduction. Springer-Verlag, Berlin Heidelberg.

Rosenkranz, P., Brüggemann, N., Papen, H., Xu, Z., Horvath, L., Butterbach-Bahl, K., 2006. Soil N and C trace gas fluxes and microbial soil N turnover in a sessile oak (Quercus petraea (Matt.) Liebl.) forest in Hungary. Plant Soil 286, 301–322.

Rumelhart, D.E., Hinton, G.E., Williams, R.J., 1986. Learning representations by back-propagating errors. Nature 323, 533–536.

Seinfeld, J.H., Pandis, S.N., 1997. Atmospheric Chemistry and Physics, from Air Pollution to Climate Change. John Wiley & Sons, New York, pp. 1326.

Sintermann, J., Dietrich, K., Häni, C., Bell, M., Jocher, M., Neftel, A., 2016. A miniDOAS instrument optimised for ammonia field measurements. Atmos. Meas. Technol. 9, 2721–2734. https://doi.org/10.5194/amt-9-2721-2016.

Song, B., Sun, J., Zhou, Q., Zong, N., Li, L., Niu, S., 2017. Initial shifts in nitrogen impact on ecosystem carbon fluxes in an alpine meadow: patterns and causes. Biogeosciences 14, 3947–3956.

Spirig, C., Flechard, C.R., Ammann, C., Neftel, A., 2010. The annual ammonia budget of fertilised cut grassland – Part 1: micrometeorological flux measurements and emissions after slurry application. Biogeosciences 7, 521–536.

Sutton, M.A., Tang, Y.S., Miners, B., Fowler, D., 2001. A new diffusion denuder system for long-term regional monitoring of atmospheric ammonia and ammonium. Water Air Soil Pollut. Focus 1, 145–156.

Sutton, M.A., Nemitz, E., Theobald, M.R., Milford, C., Dorsey, J.R., Gallagher, M.W., Hensen, A., Jongejan, P.A.C., Erisman, J.W., Mattsson, M., Schjoerring, J.K., Cellier, P., Loubet, B., Roche, R., Neftel, A., Hermann, B., Jones, S.K., Lehman, B.E., Horvath, L., Weidinger, T., Rajkai, K., Burkhardt, J., Löpmeier, F.J., Daemmgen, U., 2009. Dynamics of ammonia exchange with cut grassland: strategy and implementation of the GRAMINAE integrated experiment. Biogeosciences 6, 309–331.

Sutton, M.A., Howard, C.M., Erisman, J.W., Billen, G., Bleeker, A., Grennfelt, P., van Grinsven, H., Grizzetti, B., 2011. The European Nitrogen Assessment: Sources, Effects, and Policy Perspectives. Cambridge University Press, Cambridge, UK.

Sutton, M.A., Reis, S., Riddick, S.N., Dragosits, U., Nemitz, E., Theobald, M.R., Tang, Y.S., Braban, C.F., Vieno, M., Dore, A.J., Mitchell, R.F., Wanless, S., Daunt, F., Fowler, D., Blackall, T.D., Milford, C., Flechard, C.R., Loubet, B., Massad, R., Cellier, P., Personne, E., Coheur, P.F., Clarisse, L., Van Damme, M., Ngadi, Y., Clerbaux, C., Skjøth, C.A., Geels, C., Hertel, O., Wichink Kruit, R.J., Pinder, R.W., Bash, J.O., Walker, J.T., Simpson, D., Horváth, L., Misselbrook, T.H., Bleeker, A., Dentener, F., de Vries, W., 2013. Towards a climate-dependent paradigm of ammonia emission and deposition. Phil. Trans. Biol. Sci. 368, 20130166.

Tang, Y.S., Simmons, I., van Dijk, N., Di Marco, C., Nemitz, E., Dämmgen, U., Gilke, K., Djuricic, V., Vidic, S., Gliha, Z., Borovecki, D., Mitosinkova, M., Hanssen, J.E., Uggerud, T.H., Sanz, M.J., Sanz, P., Chorda, J.V., Flechard, C.R., Fauvel, Y., Ferm, M., Perrino, C., Sutton, M.A., 2009. European scale application of atmospheric reactive nitrogen measurements in a low-cost approach to infer dry deposition fluxes. Agric. Ecosyst. Environ. 133, 183–195.

Thoene, B., Rennenberg, H., Weber, P., 1996. Absorption of atmospheric NO_2 by spruce (Picea abies) trees. II. Parameterization of NO2 fluxes by controlled dynamic chamber experiments. New Phytol. 134, 257–266.

von Bobrutzki, K., Braban, C.F., Famulari, D., Jones, S.K., Blackall, T., Smith, T.E.L., Blom, M., Coe, H., Gallagher, M., Ghalaieny, M., McGillen, M.R., Percival, C.J., Whitehead, J.D., Ellis, R., Murphy, J., Mohacsi, A., Pogany, A., Junninen, H., Rantanen, S., Sutton, M.A., Nemitz, E., 2010. Field inter-comparison of eleven atmospheric ammonia measurement techniques. Atmos. Meas. Technol. 3, 91–112.

Webb, E.K., Pearman, G.I., Leuning, R., 1980. Correction of flux measurements for density effects due to heat and water vapor transfer. Q. J. R. Meteorol. Soc. 106, 85–100.

Wentworth, G.R., Murphy, J.G., Benedict, K.B., Bangs, E.J., Collett Jr., J.L., 2016. The role of dew as a night-time reservoir and morning source for atmospheric ammonia. Atmos. Chem. Phys. 16, 7435–7449. https://doi.org/10.5194/acp-16-7435-2016.

WHO, 2006. WHO Air Quality Guidelines for Particulate Matter, Ozone, Nitrogen Dioxide and Sulphur Dioxide, Global Update 2005: Summary of Risk Assessment. World Health Organization, Geneva, Switzerland.

Wolff, V., Trebs, I., Foken, T., Meixner, F.X., 2010. Exchange of reactive compounds: concentrations and fluxes of total ammonium and total nitrate above a spruce canopy. Biogeosciences 7, 1729–1744.

Wutzler, T., Lucas-Moffat, A., Migliavacca, M., Knauer, J., Sickel, K., Šigut, L., Menzer, O., Reichstein, M., 2018. Basic and extensible post-processing of eddy covariance flux data with REddyProc. Biogeosciences 15 (16), 5015–5030.

Wyers, P.G., Erisman, J.W., 1998. Ammonia exchange over coniferous forest. Atmos. Environ. 32, 441–451.

Zöll, U., Brümmer, C., Schrader, F., Ammann, C., Ibrom, A., Flechard, C.R., Nelson, D.D., Zahniser, M., Kutsch, W.L., 2016. Surface–atmosphere exchange of ammonia over peatland using QCL-based eddy-covariance measurements and inferential modeling. Atmos. Chem. Phys. 16, 11283–11299.